Journal of Advanced Research in Fluid Mechanics and Thermal Sciences

Journal homepage:
https://semarakilmu.com.my/journals/index.php/fluid_mechanics_thermal_sciences/index
ISSN: 2289-7879

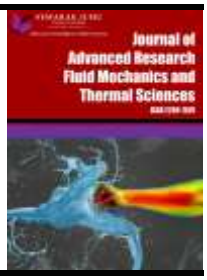

Effect of Multi-Cycle Combustion on Nox Emission Formation of Hydrogen Fuel in Pulse Detonation Engine

Mahammadsalman Warimani[1], Sayed Ahmed Imran Bellary[2], Muhammad Hanafi Azami[3], Sher Afghan Khan[3,*], Sonachalam Muthuswamy[2], Manieniyan Veerasigamani[4]

[1] Department of Mechanical Engineering, P.A.College of Engineering, Mangalore, Karnataka, India
[2] Department of Mechanical Engineering, Arvind Gavali College of Engineering, Satara, Maharashtra, India
[3] Department of Mechanical Engineering, International Islamic University Malaysia (IIUM), Kuala Lumpur, Malaysia
[4] Department of Mechanical Engineering, Annamalai University, India

ARTICLE INFO

Article history:
Received 15 April 2024
Received in revised form 17 July 2024
Accepted 29 July 2024
Available online 15 August 2024

Keywords:
Pulse detonation engine; emission; EINOx; CFD; hydrogen fuel

ABSTRACT

Pulse Detonation Engines (PDE) have higher temperature combustion, which results in higher Nitrogen Oxides (NOx) emissions. The current study will investigate the formation of NOx using the computational fluid dynamics (CFD) method for multi-cycle combustion processes. The CFD model is created by varying the boundary conditions for hydrogen fuel. According to the CFD simulation, the maximum value of Nitrous oxide produced was 27000 ppm in the middle of the combustion tube during the first cycle, with a minimum range of 0-20 ppm produced at the start and end of both cycles. The computed results of a maximum rate of Nitrous Oxide of 100 microseconds are consistent with previous literature. In the PDE analytical analysis, hydrogen fuel had the highest Emission Index of Nitrous Oxide (EINOx) of 58.64 g/kg of fuel, and methane fuel had the lowest EINOx of 10.06 g/kg. In CFD analysis at 10 microseconds, RAM-jets produced around 100 g/kg of fuel, while PDE produced 50 g/kg of fuel in EINOx.

1. Introduction

During a detonation, a few thousand meters per second supersonic combustion wave moves about an unburned fuel/air combination. Detonation produces enormous overpressures and is a far more intense process than deflagration. Pulse detonation combustion (PDC), one of the early ideas in Pressure Gain Combustion (PGC), was first proposed by Zel'dovich and is still being researched as an alternate combustion technique for use in aviation and power generation [1]. Many methods are used to reduce NOx emissions caused by high pressure and temperature inside the combustion chamber [2]. The pulse detonation approach was considered reserved for supersonic aircraft only in the 1950s. PDE's contaminants have only been the subject of a few investigations. First, the gas cycles used detonations to provide up to 10% more power for thermodynamic efficiency [3,4].

* *Corresponding author.*
E-mail address: sakhan@iium.edu.my

https://doi.org/10.37934/arfmts.120.1.217233

When combustion occurs at extremely high pressure and temperature, it generates a detonation wave, which results in NO accumulation. The two-dimensional PDE model with 12-species and 28-step H_2/O_2/NOx chemical kinetics produces relatively more NOx [5,6]. The pollutant from a multi-step chemical reactor is assessed using a post-processing tool [7,8].

The principal cause of thermal NOx is the combustion temperature [9]. The combustion temperature rises due to increased thermal efficiency, which enhances NOx production [10,11]. As a result, the equivalence ratio (lean or rich mixtures) and residence period significantly impact the NOx emission parameter [12].

The most recent work by Xisto *et al.,* [13] focused on calculating the CO_2 and NOx emissions of an optimized geared inter-cooled PDC turbofan engine, and it was discovered that detonation in lean mixes allowed for a significant decrease in NOx emission. Djordjevic *et al.,* [10] and Hanraths *et al.,* [14] investigated the two NOx emission reduction strategies. Both strategies outperform the use of lean mixes. They also studied the effect of operating frequency, fill time, sampling duration, and probe geometry on NOx production. The findings indicate that gas sampling is a difficult task in unstable combustion. Yungster and Breisacher [15] investigated the shortest potential detonation tubes. The results show that using lean or rich mixtures reduces NOx production in Jet-A-fueled PDEs. Using Euler equations, Yungster *et al.,* [16] examined NOx production in axisymmetric hydrogen-filled PDE. NO concentrations are kept to a minimum at specific operating frequencies and fuel-air ratios. However, changes in the fuel-air ratio and residence time significantly impact NOx formation [17]. The results show that stoichiometric mixtures produce more NOx.

Schauer *et al.,* [18] investigated the exhaust emissions of a hydrogen-air mixture with a fuel-air ratio ranging from 0.7 to 1.3 and an ethylene-air mixture with a fill fraction ranging from 0.2 to 1. They discovered NOx concentrations ranging from 2500 ppm to 100 ppm. Carbon monoxide emissions ranged from 25,000 ppm to 3000 ppm.

In aerospace technology, hydrogen fuel remains a potential renewable energy importer [19]. Because hydrogen has a lower molecular weight, higher reactivity, and higher specific heat, it performs better in PDEs [20,21]. Furthermore, the hydrogen-air mixture transitions more easily from deflagration to detonation than most other fuel-air mixtures. These characteristics indicate that a hydrogen-air mixture is the most practical material for shock-focusing direction initiation.

One-dimensional simulations are the most computationally efficient [22,23]. They cannot, however, give precise multidimensional flow dynamics or be used to solve PDE problems more precisely [24]. Warimani *et al.,* [25] investigated the effect of different hydro-blended fuels on the performance of a pulse detonation engine (PDE) analytically and computationally. They discovered that hydrogen blended with methane and kerosene fuels suits PDE use. However, hydrogen has the highest specific impulse at an equivalence ratio of one [26]. According to the available literature, pollutant emission characteristics, particularly NOx, have not received as much attention as other areas of PDE during the development of innovative combustion concepts such as PDC. The authors have now studied the formation of NOx exhaust emissions in multidimensional PDE and explained the combustion kinetics at high pressure and high temperature [27]. As a result, the current study's objective, two-dimensional numerical simulations, is performed to analyze the effect of NOx emission multi-cycle PDE for hydrogen fuel.

2. Methodology

2.1 Governing Equation for Multi-Cycle Pulse Detonation Engine

Understanding the intricate reactive flow field within the PDE throughout the entire cycle is crucial. Numerous researchers have examined the PDE cycle in one, two, and theoretically [28].

ANSYS Fluent software simulates the multi-cycle PDE tube's numerical models. The unsteady two-dimensional Reynolds-Averaged Navier-Stokes (URANS) equations are implemented in finite volume for the simulation. Due to the flame's supersonic characteristics, the Arrhenius kinetic expressions are used to calculate the finite-rate reactions, and a laminar finite-rate model is chosen concurrent resolution of the variables allowed for faster solution convergence to the implicit formulation in each computing cell [20].

Analysis of multi-cycle combustion phenomena in two-dimensional PDE requires the solution of the governing equations continuity, momentum, and energy using state equations for independent variables [28-30]. By changing the boundary conditions for hydrogen fuel, a model is built. It uses a transient Shear Stress Transport (SST) Turbulence Kinetic Energy (K) - turbulent dissipation rate (ε) model.

Continuity equation

$$\frac{\partial \rho}{\partial t}+\frac{\partial}{\partial x_i}\left(\rho u_i\right)=0 \tag{1}$$

Momentum equation

$$\frac{\partial}{\partial t}\left(\rho u_i\right)+\frac{\partial}{\partial x_i}\left(\rho u_i u_j\right)=-\frac{\partial P}{\partial x_i}+\frac{\partial \tau_{ij}}{\partial x_i} \tag{2}$$

Where τ_{ij} is the viscous stress tensor

$$\tau_{ij}=\mu\left(\frac{\partial u_i}{\partial x_j}+\frac{\partial u_j}{\partial x_i}-\frac{2}{3}\delta_{ij}\frac{\partial u_i}{\partial x_i}\right) \tag{3}$$

Energy equation

$$\frac{\partial}{\partial t}\left[\rho\left(e+\frac{1}{2}u_i u_i\right)\right]+\frac{\partial}{\partial x_j}\left[\rho u_i\left(h+\frac{1}{2}u_i u_i\right)\right]=\frac{\partial}{\partial x_j}\left(u_i \tau_{ij}\right)-\frac{\partial q_j}{\partial x_j} \tag{4}$$

and

$$h=e+P/\rho \tag{5}$$

Turbulence Model

The realizable k-ε turbulence model based on transport equations of turbulent kinetic energy (k) and dissipation rate (ε):

$$\frac{\partial}{\partial t}(\rho k)+\frac{\partial}{\partial x_j}(\rho k u_j)=\frac{\partial}{\partial x_j}\left[\left(\mu+\frac{\mu_t}{\sigma_k}\right)\frac{\partial k}{\partial x_j}\right]+P_k+P_b-\rho\varepsilon-Y_M+S_k \tag{6}$$

and

$$\frac{\partial}{\partial t}(\rho\varepsilon)+\frac{\partial}{\partial x_j}(\rho\varepsilon u_j)=\frac{\partial}{\partial x_j}\left[\left(\mu+\frac{\mu_t}{\sigma_\varepsilon}\right)\frac{\partial\varepsilon}{\partial x_j}\right]+\rho C_1 S\varepsilon-\rho C_2\frac{\varepsilon^2}{k+\sqrt{\nu\varepsilon}}+C_{1\varepsilon}\frac{\varepsilon}{k}C_{3\varepsilon}P_b+S_\varepsilon \tag{7}$$

where, $C_1=\max\left[0.43,\frac{\eta}{\eta+5}\right]$, $\eta=S\frac{k}{\varepsilon}$, $S=\sqrt{2S_{ij}}S_{ij}$.

where P_k and P_b represent the generation of turbulence kinetic energy due to the mean velocity gradient and due to buoyancy, respectively, and σ_κ and σ_ε are the turbulent Prandtl numbers for *k* and ε.

Species transport equation

The transport equation for the mass fraction of i^{th} species is given by Alam *et al.,* [29].

$$\frac{\partial}{\partial t}\left(\rho Y_i\right)+\frac{\partial}{\partial x_j}\left(\rho u_j Y_i\right)=\frac{\partial}{\partial x_j}\left(\rho D_{ij}\frac{\partial Y_i}{\partial x_j}\right)+R_i+S_i \tag{8}$$

Here, *c* is the concentration of chemical species, u_i velocity, diffusion coefficient, and S is the source term.

The transport coefficients should be calculated using the gas kinetic theory [30,31]. The binary diffusion coefficients are expressed as,

$$D_{ij}=\frac{3}{8}\frac{\sqrt{2\pi k_{th}Tm_i\,m_j/\left(m_i+m_j\right)}}{\pi\sum_{ij}^{2}\Omega^{(1,1)}(T_{ij}^{*})}\frac{1}{\rho} \tag{9}$$

and the coefficient of thermal conductivity k_{th} is

$$k_{th}=\frac{1}{2}\left[\sum_i\alpha_i k_i+\left(\sum_i\frac{\alpha_i}{k_i}\right)^{-1}\right] \tag{10}$$

where, $T_{ij}^{*}=kT/\sqrt{\varepsilon_i^{*}\varepsilon_j^{*}}$, and $k_i=\mu_i C_{pi}/\mathrm{Pr}$ (11)

k_i is the heat conduction coefficient of the i^{th} species, ε_i^{*} is the constant of Lennard–Jones potential expression, and Pr is the Prandtl number varying from 0.71-0.75.

Chemical Kinetics Model

The turbulent reaction rate in combustion systems can be calculated using the generalized Finite-rate/Eddy-dissipation formulation.

Let us consider that the general form of r^{th} reaction can be written as

$$\sum_{i=1}^{n} \nu_{i,r}^{'} M_i \Leftrightarrow \sum_{i=1}^{n} \nu_{i,r}^{''} M_i \tag{12}$$

The molar rate of species *i* can be calculated by the creation and destruction rates of each r^{th} reaction.

$$\hat{R}_{i,r} = \Gamma\left(\nu_{i,r}^{''} - \nu_{i,r}^{'}\right)\left(k_{f,r}\prod_{j=1}^{nr}\left[C_{j,r}\right]^{\eta_{j,r}^{'}} - \prod_{j=1}^{nr}\left[C_{j,r}\right]^{\eta_{j,r}^{''}}\right) \tag{13}$$

$$k_{f,r} = A_r T^{\beta_r} e^{-E_r/RT} \tag{14}$$

where,

A_r = Pre-exponential factor

$\hat{R}_{i,r}$ = Arrhenius molar rate of creation/destruction of species *i* in reaction *r*

$\upsilon_{i,r}^{'}, \upsilon_{i,r}^{''}$ = The stoichiometric coefficient for reactant *i* in reaction *r*

$\eta_{j,r}^{'}, \eta_{j,e}^{''}$ = Forward and backward rate exponent for each reactant and product species *j* in reaction *r*

β_r = Temperature exponent

E_r = The activation energy for the reaction

$k_{f,r}$ = The forward rate constant of reaction r

$C_{j,r}$ = The molar concentration of species *j* in reaction *r*

2.2 Chemical Reaction Mechanisms on the Pollutant Formation

The prompt NO formation was discovered by Fenimore [17,32]. This mechanism is critical in rich conditions. However, its contribution is less than that of the thermal NO formation. The rapid NO formation is related to the interaction of atmospheric nitrogen with hydrocarbon radicals in the early stage of the flame region, which makes it different from the thermal formation sub-mechanism. In this mechanism, the interaction of atomic nitrogen with HC radicals creates amines and cyano compounds that are converted to some intermediate compounds and ultimately to NO. The formation mechanism of the prompt NO is not as simple as the thermal NO formation mechanism due to the presence of a high number of hydrocarbon radicals and different reaction paths. Still, its complexity may be reduced by considering HC radicals as the principal radicals interacting with the nitrogen and skipping the process that leads to the formation of HC. The following reactions initiate the Prompt NO formation mechanism.

$$\mathrm{CH} + \mathrm{N_2} \leftrightarrow \mathrm{HCN} + \mathrm{N} \tag{15}$$

$$\mathrm{C} + \mathrm{N_2} \leftrightarrow \mathrm{CN} + \mathrm{N} \tag{16}$$

After this point, the mechanism depends on the value of the equivalence ratio. For equivalence ratios less than 1.2, NO formation is based on the following reactions [33].

$$\mathrm{HCN} + \mathrm{O} \leftrightarrow \mathrm{NCO} + \mathrm{H} \tag{17}$$

$$NCO + H \leftrightarrow NH + CO \quad (18)$$

$$NH + H \leftrightarrow N + H_2 \quad (19)$$

$$N + OH \leftrightarrow NO + H \quad (20)$$

The mechanism is too complex to present richer conditions in a few elementary reactions. Implementing the prompt, NO formation in a fuel combustion mechanism requires a set of elementary reactions representing a complex interaction between the hydrocarbon and nitrogen species. Since these elementary reactions do not show up in a simplified combustion mechanism (especially those based on the Pyrolysis process), rapid NO formation should be implemented in a simple combustion mechanism.

2.3 Effect of Initial Conditions

Table 1 shows the detonation velocity for all selected fuels and initial conditions. Hydrogen fuel requires low ignition energy, and it has high flame speed. Because of these properties, also in small-size tubes, it can produce a higher velocity value. In our investigation, 12 cm and 20 cm tubes are selected for detonation combustion. In a 12 cm tube size, kerosene fuel failed to achieve detonation velocity and other thermodynamic properties. This research investigates the requirement for a minimum 20 cm tube for kerosene fuel to produce detonation. In the direct initiation method, spark size is vital in generating detonation velocity. As shown in Table 1, despite having a high temperature of 2500 K and 60 bar, kerosene failed to generate the required velocity because its spark gap was lower than the other two kerosene combinations. A minimum spark zone size of 3.5 % (0.035 of length) is required to generate the ideal detonation velocity of kerosene.

On the other hand, hydrogen requires only 0.5 % (0.005 of length) of the length of the spark zone to generate detonation velocity. This research shows that hydrogen 30 bar pressure, 2500 K temperature, and spark gap of 0.5 % of length produced accurate results compared with NASA CEA and available literature. Meanwhile, kerosene 60 bar pressure, 2000 K temperature, and spark gap of 3.5 % of Length produced accurate results compared with available literature.

Table 1
Variation of detonation velocity for selected fuel and variation of initial conditions

Fuel	Pressure (Bar)	Temperature K	Length (cm)	Spark size (cm)	Detonation velocity (m/s)
Hydrogen	30	2500	12	0.06	2300
Hydrogen	20	1800	12	0.06	1900
Hydrogen	30	2500	20	0.1	1950
Kerosene	60	2500	20	0.32	350
Kerosene	60	2300	20	0.7	1300
Kerosene	60	2000	20	0.7	1400

2.4 Computational Domain

The detonating tube size selected for the analysis in the current numerical simulation is 200 mm long and 20 mm in diameter, as shown in Figure 1. In two dimensions, the geometry is axisymmetric. This geometric size is equivalent to that mentioned by Busing and Pappas [34] and Morris [35]. In these calculations, as depicted in Figure 2, a tiny spark region sets off the detonation, where extremely high pressure and temperature reasons develop. Pressure, temperature, and spark zone

size varied during the simulation's early stages until a detonation wave was produced. Because the PDE geometry is symmetrical about the x-axis, this research will only focus on the upper half of the geometry.

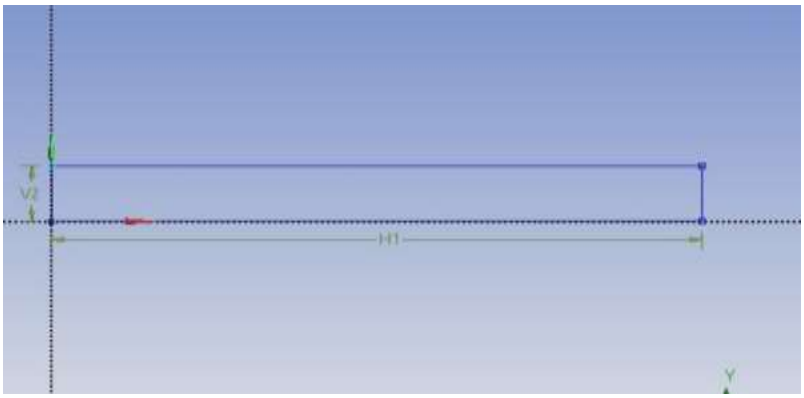

Fig. 1. Model geometry created using ANSYS software

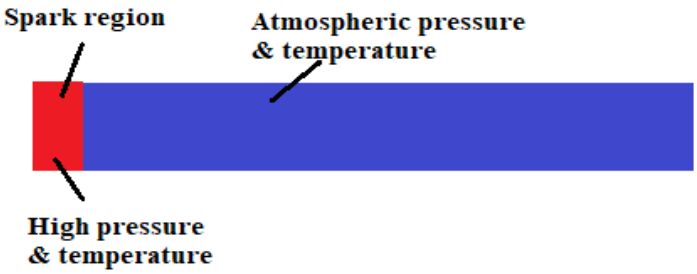

Fig. 2. High pressure and temperature patch

2.5 Mesh Generation

Ansys software is used for mesh generation. The detonation tube study was initiated with 40,000 elements to save computational time. The eliminated error of detonation velocity would decrease as the grid size increased once the track-matching results matched those obtained in previous literature and NASA CEA [36]. Detonation velocities of 2040 m/s, 2280 m/s, and 2300 m/s are obtained with grid elements of 60,000 (mesh 1), 80,000 (mesh 2), and 1,00,000 (mesh 3), respectively. Compared to the 80000 elements shown in Table 2, the grid element with the lowest detonation velocity error is 0.1 million. As a result, the simulation results presented in this paper for 0.1 million grid elements. When mesh one and two are used, the error in detonation velocity is 10.52%. Mesh 3 is thus considered to reduce the error percentage. Meshes 2 and 3 have an error percentage of 0.86%, significantly lower than the error percentage of mesh 1. Finally, it was agreed that a mesh 3 with 0.1 million elements was appropriate for numerical simulation.

Table 2
Detonation velocity analysis concerning previous works

Detonation velocity (m/s)	Mesh Element (Million)	Error (%)
2040	0.06	14
2280	0.08	4.2
2300	0.1	3.3

2.6 Initial and Boundary Conditions of Multi-cycle Analysis

The regional flow conditions govern the boundary conditions of the detonation tube, and multi-cycle analysis differs from a single cycle, as presented in Table 3 [37]. The head end is portrayed as a stiff wall when the valve is closed. Total temperature (Tt1) and pressure (Pt1) during the purging are indicated as 358 K and 1.9 bar, respectively. With the air mass fraction set at 0.226, interior point extrapolation determines the axial velocity. For a 1.2 Mach number, the beginning condition provided is appropriate [38].

The same conditions are applied during the filling stage, but the mass fractions of the reactants H_2 and O_2 are stated as 0.028 and 0.226, respectively. It is assumed that all solid walls are adiabatic. The filling velocity must be greater than the purge velocity. To avoid pre-ignition, the tube is purged. The purging process begins when the head end pressure falls below atmospheric pressure.

Table 3
Multi-cycle boundary conditions for PDE

Process	Mass fraction				Total pressure (Bar)	Total Temperature (K)
	H_2	O_2	H_2O	N_2	Pt	Tt
Filling	0.02852	0.22636	0	0.746	1.9	358
Initiation	0	0	0.25488	0.746	Wall boundary condition applied.	
Detonation	Wall boundary condition applied.					
Purging	0	0.22636	0	0.746	1.9	358

The boundary conditions of the PDE tube are shown in Figure 3. In this 2-D axisymmetric simulation, the wall and pressure outlet were the two primary forms of boundary conditions. The combustion takes place inside the combustion chamber. The right side of the combustor is viewed as open-end using a fixed pressure outlet boundary condition. The top and left sides of the tube are thought of as walls.

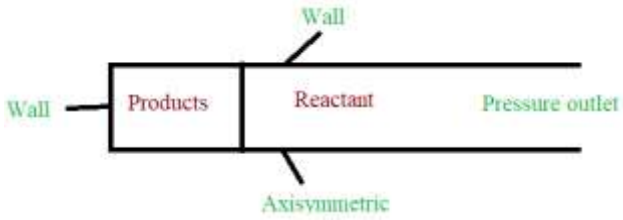

Fig. 3. PDE tube boundary conditions

In this investigation, the direct initiation approach was adopted. For simulation, the spark is situated close to the tube's closed end. If there is no detonation in the spark zone, the area, temperature, or pressure can be raised until more detonation occurs. The valve opening pattern is expected to be stepwise, that is, entirely closed or completely open. Thus, the three time periods that regulate the multi-cycle operation are the valve-closed period for detonation initiation and propagation, the blowdown of combustion products, and the open valve period for both the purge and filling periods. These three times add up to one PDE cycle time. During the close valve period, the thrust wall is considered inviscid and adiabatic. As the filling period concludes, the detonation tube is filled with a stoichiometric gas mixture, and the valve is instantly closed.

2.7 Numerical Methodology

When the equations between state and species are closely linked, a density-based solver for simulation is chosen as appropriate. A density-based solver is suitable for compressible and supersonic flow simulation.

This study employed Roe's Flux-Difference Splitting (Roe-FDS) scheme for high Mach number flows. This study compares two interpolation methods. They are first-order and second-order upwind, respectively. First-order upwind converges quickly, while second-order upwind may converge more slowly since it requires larger shapes for second-order precision, which is necessary with tri/tetra mesh or when the flow is not aligned with the grid. Conversion could be slower on a mesh or when the flow is not aligned with the grid. The conventional initialization technique is applied—the more realistic the value chosen, the better (quicker) the convergence. The step size was 10.8 seconds due to the short reaction time for detonation. Because of the minor grid size, the Courant-Friedrichs-Lewy (CFL) number was reduced to 0.6 [39]. The laminar viscous model is considered. There should be enough iterations for the solver to solve the problem.

3. Validation

The key to any effective numerical simulation of detonation caused by a shock wave focusing on a combustible mixture is accurately describing the chemical reaction and mechanical behavior of a combustible mixture at high temperature and pressure. Before presenting our results, we present the validation of current numerical methods by referring to works' temperature and species concentration distribution, as shown in Figure 4, and also a 2-dimensional axisymmetric cylinder model, as shown in Figure 5 [20]. The numerical simulation validation revealed that with the initial conditions for starting a detonation wave at 30 bar and 2500 K. Figure 5 shows that the propagating wave has a leading shock wave, an expansion wave area, and a uniform area, which agrees with the Chapman and Jouguet (C-J) model [39]. The hydrogen-air mixture reacts quickly behind the shock front. The calculated flow agrees well with the theoretical pressure, temperature, and species concentration distribution. The chosen chemical reaction model and numerical algorithm were deemed acceptable, with only minor differences in pressure, temperature, and species concentration distribution compared to previous works and a relative error of less than 13%.

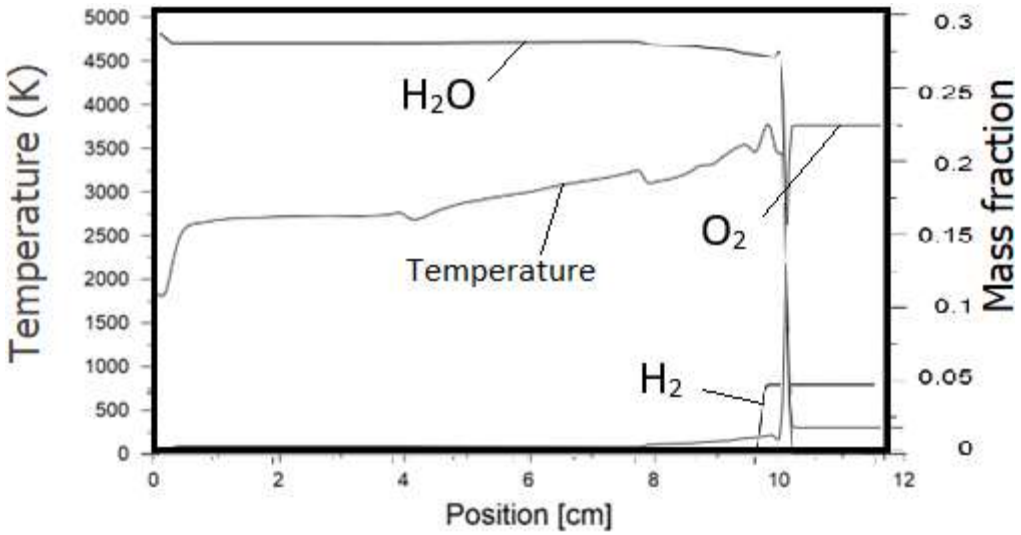

Fig. 4. The temperature and species concentration distribution of the detonation wave

4. Results and Discussions

Calculations for multiple cycles previous research has shown that single-pulse calculations differ significantly from multi-cycle analysis [40]. As a result, numerical simulations were run in this study to determine the effects of temperature on emission during multi-cycle operation. Refueling occurs when the pressure at the thrust wall drops to or below the surrounding atmospheric pressure. When the combustible mixture fills 97% of the tube, the valve closes, triggering a new detonation wave.

Figure 5 and Figure 6 depict the pressure evolution of the PDE flow field during the first and second cycles. In the first cycle, the direct initiation method starts the detonation tube. In the tube, a detonation wave takes 5 microseconds to initiate. It reaches the end of the detonation tube after 90 microseconds, and the lead shock, followed by the combustion products, continues to propagate to the atmosphere. All other processes take longer than blowing down. As shown in Figure 6, hydrogen takes approximately 75.43% of the time to reach near atmospheric conditions for pressure contour, at which point the blowdown is complete. Atmospheric pressure is reached in 550 microseconds. The tube is then purged to remove any burnt or unwanted products. The tube is cleaned during the purging process. Purging is performed for 20 microseconds by filling the tube with air. The refueling process starts at 570 microseconds and ends at 620 microseconds.

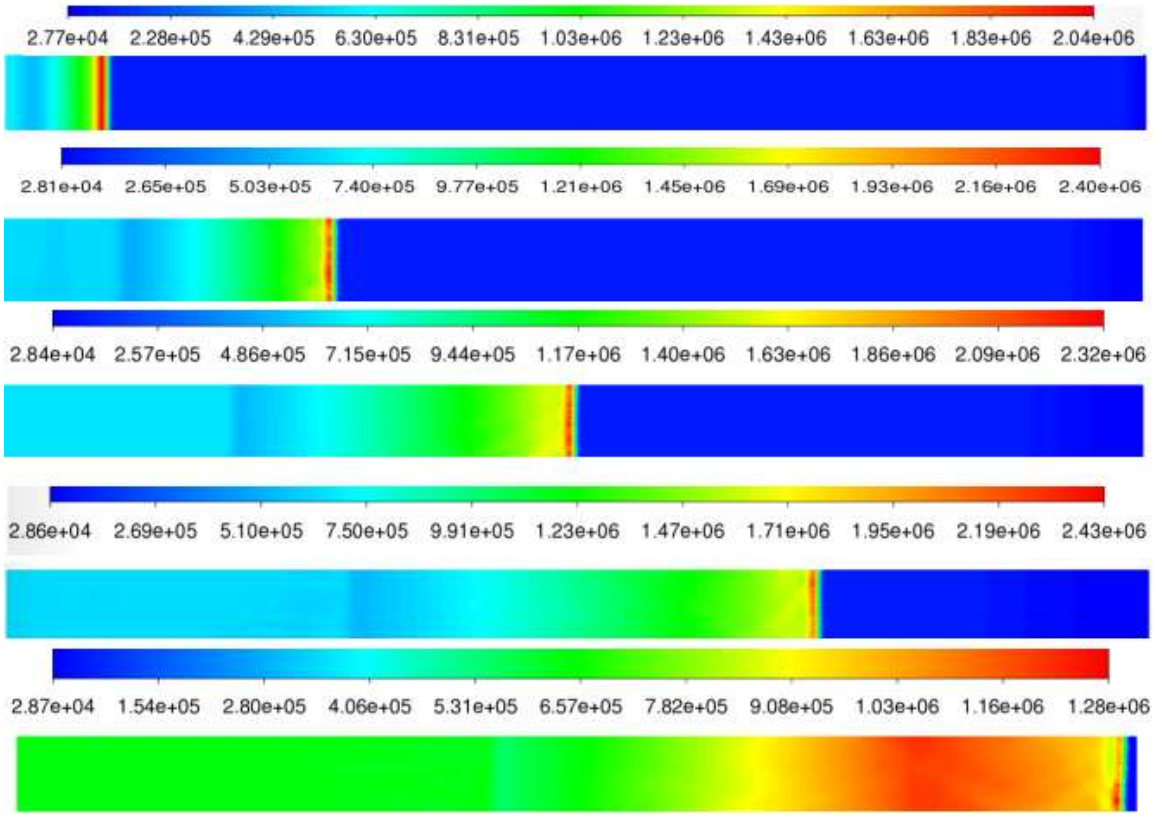

Fig. 5. The pressure evolution of the PDE flow field during the first cycle

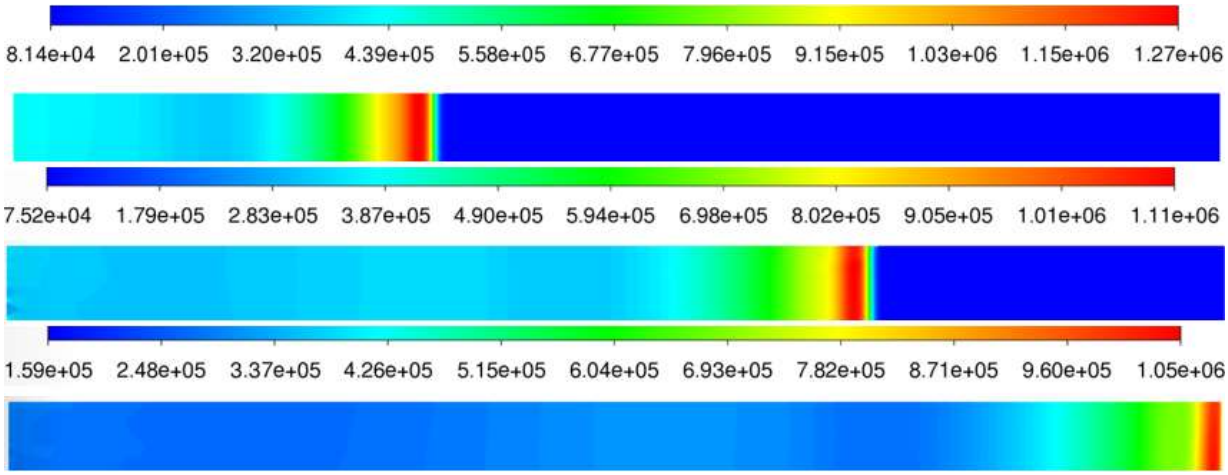

Fig. 6. Pressure evolution of the PDE flow field during the second cycle

For the duration of the initial cycle, the detonation is started using the direct initiation technique. When the pressure inside the tube approached atmospheric pressure, the second cycle began. The conditions inside the detonation tube before initiation are not uniform for the second cycle due to interactions between shock and expansion waves. This causes the detonation wave of the second cycle to propagate into mixes with irregular pressure and temperature distributions. In this study, reaching the tube end took less time than in the first cycle. It can be inferred that more cycles may be needed to establish a limit cycle behavior.

As illustrated in Figure 7, the PDE tube is evacuated until the pressure inside the tube reaches nearly 1 atm. Most researchers conducted PDE simulations only for initiation and detonation because the blowdown process takes a long time, as evidenced by this simulation work.

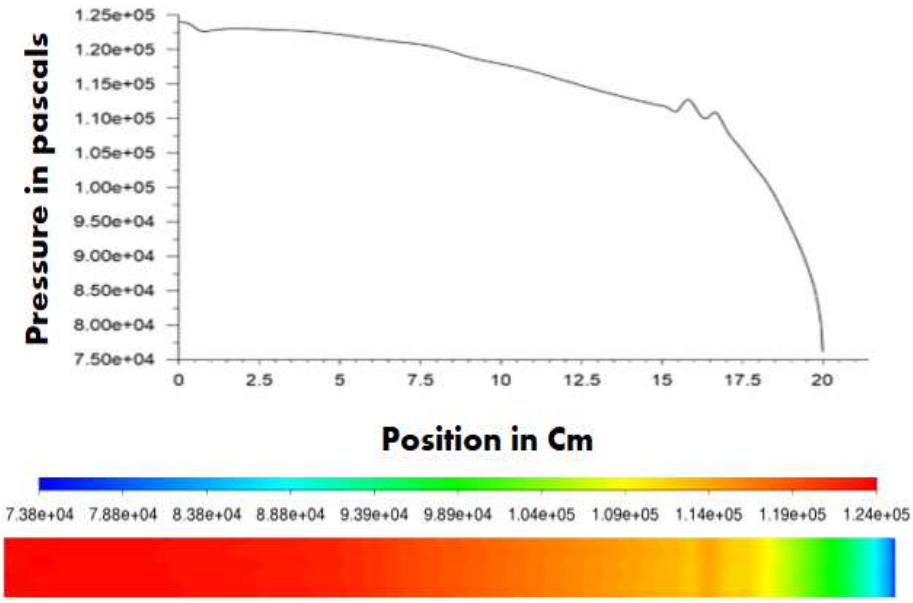

Fig. 7. Blowdown process at the end of the second cycle

Figure 8 depicts the filling of H_2 and O_2 during the filling process. For hydrogen, the mass fractions of H_2, O_2, and H_2O are 0.02852, 0.22636, and 0, respectively. Filling time should always be more significant than purging time [41]. The flow field during refueling in Figure 8 shows that the H2O mass fraction is almost zero in the tube, but a few exhaust gases remain in the center of the tube. In the investigation by Berndt and Klein [20], a small amount of exhaust gas remained in the cone's center

after refilling. According to the methodology section, these species mass fractions are computed using balancing equations.

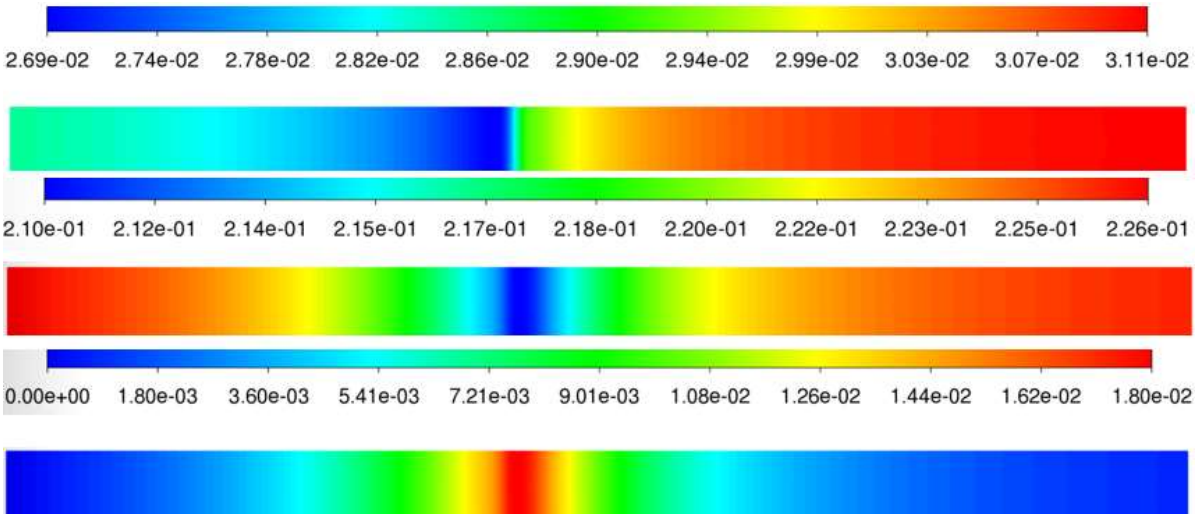

Fig. 8. Contours of species after filling for the second cycle

Figure 9 depicts the beginning of detonation in a 10-microsecond tube with a temperature of 3000 K. These temperature contour values are consistent with the findings of Berndt and Klein [20]. The temperature decreases as the detonation wave progresses, as shown in Figure 10. The maximum temperatures at the end of the first and second cycles are 3500 K and 2700 K, respectively. The amount of Emission produced is temperature dependent. As the temperature rises, so does the emission of PDE. To reduce emissions, the temperature of the PDE tube must be reduced. It is also worth noting that lowering the temperature of the PDE reduces efficiency, so it is necessary to find alternative ways to reduce engine emissions while maintaining higher efficiency.

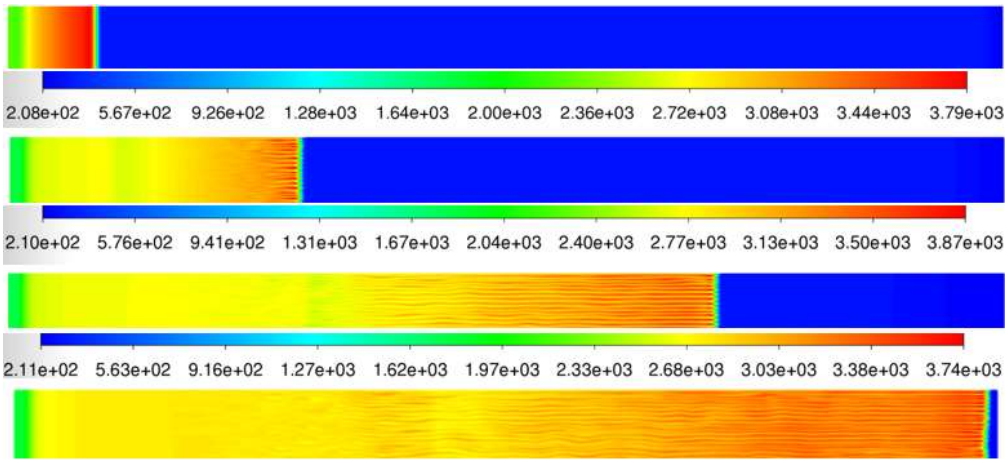

Fig. 9. Temperature distribution in the first cycle

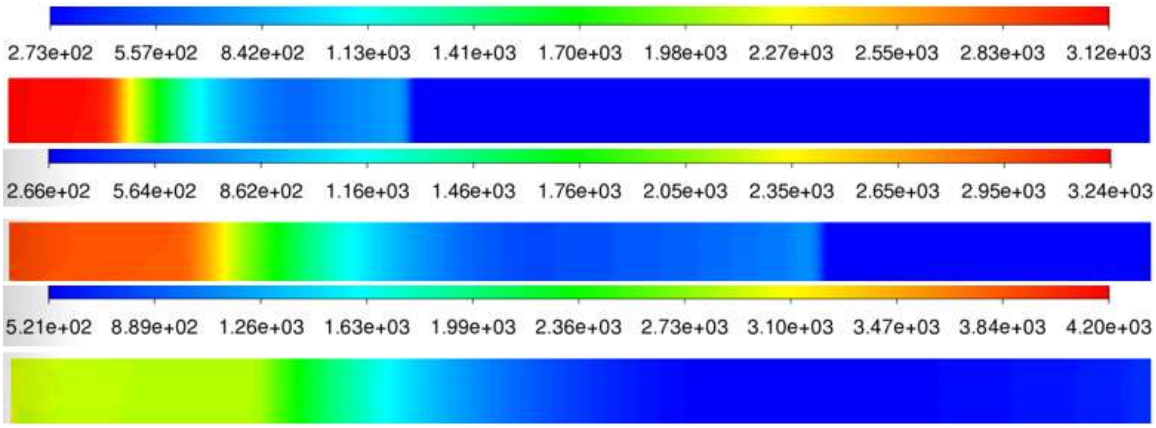

Fig. 10. Temperature distribution in the second cycle

Figure 11 depicts the time required by various processes during combustion. It is worth noting that the blowdown process consumes the most time compared to all other methods. As a result, most studies focused solely on single-cycle engine analysis.

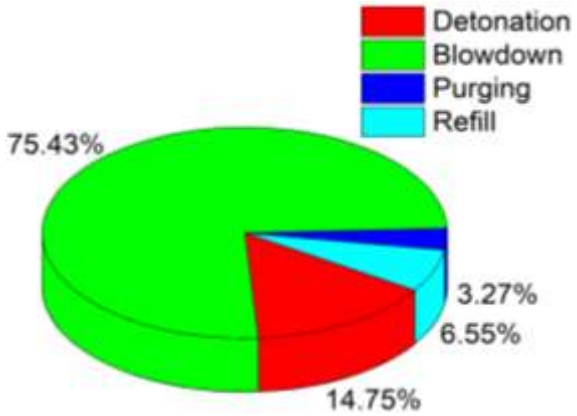

Fig. 11. Time consumed by various processes of detonation

Figure 12 depicts hydrogen's NOx- PPM variation during the first and second cycles. NOx PPM values in multi-cycle analysis are similar to those in single-cycle analysis. The exhaust has high quantities of nitrogen oxides (NOx) due to dramatically elevated combustion temperatures and pressures caused by the detonation wave [42]. The following expression can be used to calculate the thermal NO development rate.

$$\frac{d[NO]}{dt} \alpha\ k(T)[O][N_2] \tag{15}$$

where k is the reaction rate constant and varies exponentially with temperature, this is the primary regulating source of NO production in fuel-lean or rich scenarios. Temperature and the techniques utilized influence thermal emission characteristics. Because the temperature in the PDE tube was low at the start of the first cycle and at the end of the second cycle, it produced a modest amount of NOx-PPM. Because the temperature of the PDE tube increases from the middle of the first cycle to the beginning of the second cycle, the NOx-PPM value rises. It has a maximum NOx-PPM of 27000. PPM values obtained in single-cycle analysis are identical to those reported in this finding. Because of the

increased combustion temperature in the detonation tube, the simulation yields a more significant PPM value.

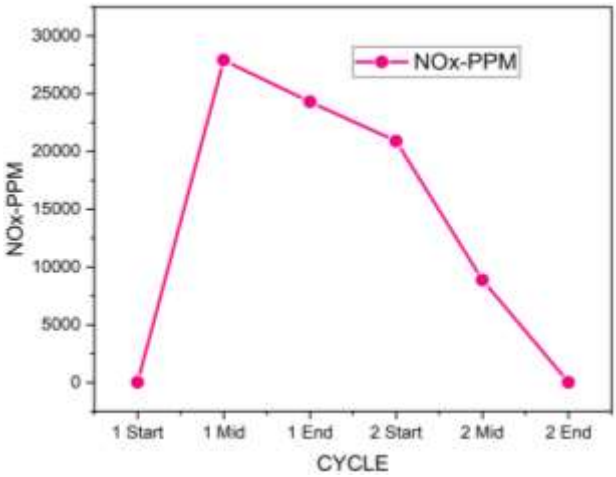

Fig. 12. Variation of NOx-PPM during the multi-cycle analysis of hydrogen

The rate of NO reaches its maximum at 100 microseconds, then swiftly drops and stays constant until the completion of the second cycle, as seen in Figure 13. This phenomenon occurs because PDE initially has a higher tube temperature, but when the temperature drops, the rate of NO also drops.

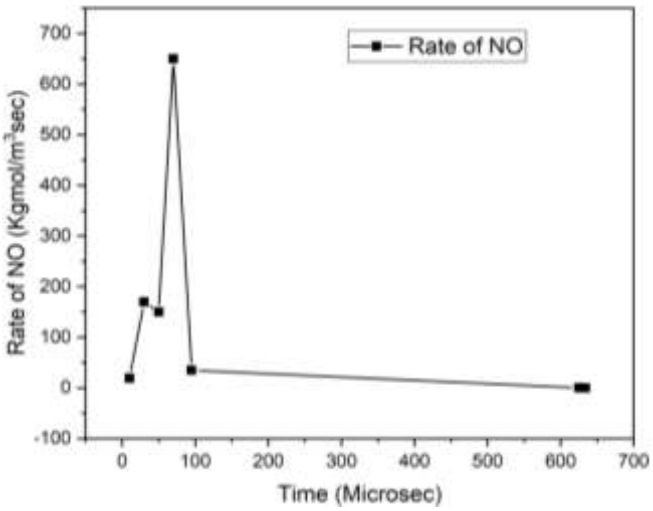

Fig. 13. Rate of NO produced during the first and second cycle

5. Conclusions

The propagation of detonation waves in a simple PDE combustor was simulated in two dimensions using CFD. In CFD, the combustion was initiated by producing a high temperature and pressure spark zone. The formation of a reflection wave was observed using pressure and temperature contours. Existing numerical and experimental results are used to benchmark the executed CFD version. The few experimental attempts to quantify NOx emissions from pulse detonation engines demonstrate that methods for reducing them must be considered. The current study considers multi-cycle analysis for NOx emission analysis for PDE for the first time. While operating in the middle of the first cycle's detonation tube, a more significant amount of NOx-PPM

was produced, as was a greater NO production rate at 100 microseconds. This critical analysis lays the groundwork for developing an advanced approach to achieving low-emission for pulse detonation engines.

Acknowledgment
This research was not funded by any grant.

References

[1] Zeldovich, Ya B. "To the question of energy use of detonation combustion." *Journal of Propulsion and Power* 22, no. 3 (2006): 588-592. https://doi.org/10.2514/1.22705
[2] Muthuswamy, Sonachalam, and Manieniyan Veerasigamani. "Comparative experimental analysis on dual fuel with biodiesel-acetylene in reactivity controlled compression ignition engine." *International Journal of Ambient Energy* 43, no. 1 (2022): 6317-6328. https://doi.org/10.1080/01430750.2021.2014958
[3] Bellini, Rafaela, and Frank K. Lu. "Exergy analysis of a hybrid pulse detonation power device." *Journal of Propulsion and Power* 26, no. 4 (2010): 875-878. https://doi.org/10.2514/1.44141
[4] Gray, J. A. T., J. Vinkeloe, J. Moeck, C. O. Paschereit, P. Stathopoulos, P. Berndt, and R. Klein. "Thermodynamic evaluation of pulse detonation combustion for gas turbine power cycles." In *Turbo Expo: Power for Land, Sea, and Air*, vol. 49767, p. V04BT04A044. American Society of Mechanical Engineers, 2016. https://doi.org/10.1115/GT2016-57813
[5] Anand, Vijay, and Ephraim Gutmark. "A review of pollutants emissions in various pressure gain combustors." *International Journal of Spray and Combustion Dynamics* 11 (2019): 1756827719870724. https://doi.org/10.1177/1756827719870724
[6] Frolov, S. M., V. Ya Basevich, V. S. Aksenov, P. A. Gusev, V. S. Ivanov, S. N. Medvedev, V. A. Smetanyuk, K. A. Avdeev, and F. S. Frolov. "Formation of nitrogen oxides in detonation waves." *Russian Journal of Physical Chemistry* B 5 (2011): 661-663. https://doi.org/10.1134/S1990793111040166
[7] Roy, Arnab, and Don Ferguson. "A physics based reactor network model of a rotating detonation engine combustor." In *Turbo Expo: Power for Land, Sea, and Air*, vol. 56697, p. V04BT04A065. American Society of Mechanical Engineers, 2015. https://doi.org/10.1115/GT2015-44055
[8] Reddy, Yeddula Rameswara, and Donti Ratnam Srinivasan. "Activation energy, Rotational and Hall current Effects of Magnetohydrodynamic 3D flow of Non-Newtonian Hybrid Nanofluid over a Stretched Plate." *Journal of Advanced Research in Numerical Heat Transfer* 20, no. 1 (2024): 36-52. https://doi.org/10.37934/arnht.20.1.3652
[9] Sonachalam, M., P. PaulPandian, and V. Manieniyan. "Emission reduction in diesel engine with acetylene gas and biodiesel using inlet manifold injection." *Clean Technologies and Environmental Policy* 22 (2020): 2177-2191. https://doi.org/10.1007/s10098-020-01968-y
[10] Djordjevic, Neda, Niclas Hanraths, Joshua Gray, Phillip Berndt, and Jonas Moeck. "Numerical study on the reduction of NOx emissions from pulse detonation combustion." *Journal of Engineering for Gas Turbines and Power* 140, no. 4 (2018): 041504. https://doi.org/10.1115/1.4038041
[11] Warimani, Mahammadsalman, Fharukh Ahmed Ghasi Mahaboobali, Sher Afghan Khan, Sonachalam Muthuswamy, and Sayed Ahmed Imran Bellary. "Numerical Investigation of NOx Reduction in a Hydrogen-Fueled Pulse Detonation Engine." *Journal of Advanced Research in Fluid Mechanics and Thermal Sciences* 114, no. 2 (2024): 106-117. https://doi.org/10.37934/arfmts.114.2.106117
[12] Yungster, Shaye, K. Radhakrishnan, and K. Breisacher. "Computational and experimental study of NOx formation in hydrogen-fueled pulse detonation engines." In *40th AIAA/ASME/SAE/ASEE Joint Propulsion Conference and Exhibit*, p. 3307. 2004. https://doi.org/10.2514/6.2004-3307
[13] Xisto, Carlos, Olivier Petit, Tomas Grönstedt, and Anders Lundbladh. "Assessment of CO_2 and NOx emissions in intercooled pulsed detonation turbofan engines." *Journal of Engineering for Gas Turbines and Power* 141, no. 1 (2019): 011016. https://doi.org/10.1115/1.4040741
[14] Hanraths, Niclas, Myles D. Bohon, Christian O. Paschereit, and Neda Djordjevic. "Gas sampling techniques for NOx emissions in pulse detonation combustion." In *AIAA Scitech 2019 Forum*, p. 1013. 2019. https://doi.org/10.2514/6.2019-1013
[15] Yungster, Shaye, and Kevin Breisacher. "Study of NOx formation in hydrocarbon-fueled pulse detonation engines." In *41st AIAA/ASME/SAE/ASEE Joint Propulsion Conference & Exhibit*, p. 4210. 2005. https://doi.org/10.2514/6.2005-4210
[16] Yungster, S., K. Radhakrishnan, and K. Breisacher. "Computational study of NOx formation in hydrogen-fuelled pulse detonation engines." *Combustion Theory and Modelling* 10, no. 6 (2006): 981-1002.

https://doi.org/10.1080/13647830600876629
[17] Adietya, Berlian Arswendo, Husein Syahab, Mochammad Nasir, Wasis Dwi Aryawan, and I. Ketut Aria Pria Utama. "Numerical Analysis into the Improvement Performance of Ducted Propeller by using Fins: Case Studies on Types B4-70 and Ka4-70." *CFD Letters* 16, no. 10 (2024): 12-42. https://doi.org/10.37934/cfdl.16.10.1242
[18] Schauer, Frederick, Royce Bradley, Viswanath Katta, and John Hoke. "Emissions in a pulsed detonation engine." In *47th AIAA Aerospace Sciences Meeting including the New Horizons Forum and Aerospace Exposition*, p. 505. 2009. https://doi.org/10.2514/6.2009-505
[19] Cecere, D., E. Giacomazzi, and Antonella Ingenito. "A review on hydrogen industrial aerospace applications." *International Journal of Hydrogen Energy* 39, no. 20 (2014): 10731-10747. https://doi.org/10.1016/j.ijhydene.2014.04.126
[20] Berndt, Phillip, and Rupert Klein. "Modeling the kinetics of the Shockless Explosion Combustion." *Combustion and Flame* 175 (2017): 16-26. https://doi.org/10.1016/j.combustflame.2016.06.029
[21] Burke, Michael P., Marcos Chaos, Yiguang Ju, Frederick L. Dryer, and Stephen J. Klippenstein. "Comprehensive H_2/O_2 kinetic model for high-pressure combustion." *International Journal of Chemical Kinetics* 44, no. 7 (2012): 444-474. https://doi.org/10.1002/kin.20603
[22] Sonachalam, M., and V. Manieniyan. "Optimization of critical angle, distance and flow rate of secondary fuel injection in DI diesel engine using computational fluid dynamics." *SN Applied Sciences* 3 (2021): 1-13. https://doi.org/10.1007/s42452-020-04138-3
[23] Suksuwan, Wasu, and Makatar Wae-hayee. "Enhancing Combustion Efficiency in Combustion Chamber: A Comparative Study of Single and Double Tangential Inlet Configurations." *Journal of Advanced Research in Numerical Heat Transfer* 16, no. 1 (2024): 70-81. https://doi.org/10.37934/arnht.16.1.7081
[24] Mohanraj, Rajendran, and Charles Merkle. "A numerical study of pulse detonation engine performance." In *38th Aerospace Sciences Meeting and Exhibit*, p. 315. 2000. https://doi.org/10.2514/6.2000-315
[25] Warimani, Mahammadsalman, Muhammad Hanafi Azami, Sher Afghan Khan, Ahmad Faris Ismail, Sanisah Saharin, and Ahmad Kamal Ariffin. "Internal flow dynamics and performance of pulse detonation engine with alternative fuels." *Energy* 237 (2021): 121719. https://doi.org/10.1016/j.energy.2021.121719
[26] Warimani, Mahammadsalman, Muhammad Hanafi Azami, Sher Afghan Khan, Ahmad Faris Ismail, Sanisah Saharin, Ahmad Kamal Ariffin, and Vijaykumar Chavan. "Analytical Assessment of Blended Fuels for Pulse Detonation Engine Performance." *Journal of Advanced Research in Fluid Mechanics and Thermal Sciences* 93, no. 2 (2022): 1-16. https://doi.org/10.37934/arfmts.93.2.116
[27] Klippenstein, Stephen J., Mark Pfeifle, Ahren W. Jasper, and Peter Glarborg. "Theory and modeling of relevance to prompt-NO formation at high pressure." *Combustion and Flame* 195 (2018): 3-17. https://doi.org/10.1016/j.combustflame.2018.04.029
[28] Hishida, Manabu, Toshi Fujiwara, and Sho-ichi Ito. "A Multi-Cycle CFD Analysis of Oxyhydrogen Pulse Detonation Engine." In *44th AIAA Aerospace Sciences Meeting and Exhibit*, p. 557. 2006. https://doi.org/10.2514/6.2006-557
[29] Alam, Noor, K. K. Sharma, and K. M. Pandey. "Numerical investigation of flame propagation and performance of obstructed pulse detonation engine with variation of hydrogen and air." *Journal of the Brazilian Society of Mechanical Sciences and Engineering* 41, no. 11 (2019): 502. https://doi.org/10.1007/s40430-019-2024-0
[30] Warnatz, Jürgen, Ulrich Maas, Robert W. Dibble, Jürgen Warnatz, Ulrich Maas, and Robert W. Dibble. "Formation of nitric oxides." *Combustion: Physical and Chemical Fundamentals, Modeling and Simulation, Experiments, Pollutant Formation* (2001): 237-256. https://doi.org/10.1007/978-3-662-04508-4_17
[31] Alam, Noor, K. K. Sharma, and K. M. Pandey. "Numerical investigation of flame propagation in pulse detonation engine with variation of obstacle clearance." *Journal of Thermal Analysis and Calorimetry* 140, no. 5 (2020): 2485-2495. https://doi.org/10.1007/s10973-019-08948-5
[32] Rezvani, Reza. "A conceptual methodology for the prediction of engine emissions." *PhD diss., Georgia Institute of Technology*, 2010.
[33] Turns, Stephen. *An Introduction to combustion concepts and applications*. McGraw-Hill, 2011.
[34] Bussing, Thomas, and George Pappas. "An introduction to pulse detonation engines." In *32nd Aerospace Sciences Meeting and Exhibit*, p. 263. 1994. https://doi.org/10.2514/6.1994-263
[35] Morris, C. I. "Numerical modeling of single-pulse gasdynamics and performance of pulse detonation rocket engines." *Journal of Propulsion and Power* 21, no. 3 (2005): 527-538. https://doi.org/10.2514/1.7875
[36] Schwer, Douglas, and Kailas Kailasanath. "Numerical investigation of the physics of rotating-detonation-engines." *Proceedings of the Combustion Institute* 33, no. 2 (2011): 2195-2202. https://doi.org/10.1016/j.proci.2010.07.050
[37] Fan, Wei, Jianling Li, Qiang Li, and Chuanjun Yan. "Numerical investigation on multi-cycle operation of pulse detonation rocket engine." *International Journal of Turbo and Jet Engines* 25, no. 3 (2008): 189-196. https://doi.org/10.1515/TJJ.2008.25.3.189
[38] Ma, Fuhua, Jeong-Yeol Choi, and Vigor Yang. "Propulsive performance of airbreathing pulse detonation engines."

Journal of Propulsion and Power 22, no. 6 (2006): 1188-1203. https://doi.org/10.2514/1.21755
[39] Saif, Mohamed, Wentian Wang, Andrzej Pekalski, Marc Levin, and Matei I. Radulescu. "Chapman-Jouguet deflagrations and their transition to detonation." *Proceedings of the Combustion Institute* 36, no. 2 (2017): 2771-2779. https://doi.org/10.1016/j.proci.2016.07.122
[40] Yungster, Shaye. "Analysis of nozzle and ejector effects on pulse detonation engine performance." In *41st Aerospace Sciences Meeting and Exhibit*, p. 1316. 2003. https://doi.org/10.2514/6.2003-1316
[41] Alam, Noor, Kaushal Kumar Sharma, and Krishna Murari Pandey. "Effects of Various Compositions of the Fuel-Air Mixture on the Pulse Detonation Engine Performance." *Combustion, Explosion, and Shock Waves* 55, no. 6 (2019): 708-717. https://doi.org/10.1134/S0010508219060121
[42] Garan, Niclas, and Neda Djordjevic. "Experimental and low-dimensional numerical study on the application of conventional NOx reduction methods in pulse detonation combustion." *Combustion and Flame* 233 (2021): 111593. https://doi.org/10.1016/j.combustflame.2021.111593